JOURNAL OF PROPULSION AND POWER
Vol. 18, No. 2, March–April 2002

Numerical Simulations of the Slingatron

G. R. Cooper*
U.S. Army Research Laboratory, Aberdeen Proving Ground, Maryland 21005-5066
D. A. Tidman†
Advanced Launch Corporation, McLean, Virginia 22101
and
M. L. Bundy‡
U.S. Army Research Laboratory, Aberdeen Proving Ground, Maryland 21005-5066

The slingatron mass accelerator is described for several track configurations (shapes) and numerical simulations of an accelerating mass traversing a given track configuration. The sled is modeled as a point mass that interacts with the slingatron track by a conventional and a new empirical velocity-dependent friction law. The closed-loop circular slingatron was found to produce high maximum sled velocities, provided the gyration angular speed is always increasing. In contrast, several spiral-shaped slingatron tracks reveal that high maximum sled velocities are obtainable with the gyration speed held constant. In fact, a slingatron constructed of semicircles is shown capable of generating high-velocity sleds in such a way that no initial sled injection is necessary. Choosing the proper initial gyration phase with an empirically determined friction model allows the mass sled to gain ever-increasing velocities when it is placed in a semicircle slingatron. The sled bearing pressure and its total acceleration are examined and presented.

Nomenclature

$\boldsymbol{A}$	=	acceleration vector
$A_{/\!/}$	=	$\boldsymbol{n}$ component of $\boldsymbol{A}$
$A_{\perp}$	=	$\boldsymbol{m}$ component of $\boldsymbol{A}$
D	=	sled diameter
$\boldsymbol{F}$	=	force vector acting on sled $F = \|\boldsymbol{F}\|$
$F_{/\!/}$	=	$\boldsymbol{n}$ component of $\boldsymbol{F}$
$F_{\perp}$	=	$\boldsymbol{m}$ component of $\boldsymbol{F}$
f	=	spin frequency of gyration vector
$\dot{f}$	=	time derivative of gyration frequency f
$\boldsymbol{i}, \boldsymbol{j}, \boldsymbol{k}$	=	Cartesian unit triad
L	=	sled length
M	=	mass of sled
$\boldsymbol{m}$	=	normal unit vector on concave side of track
$\boldsymbol{n}$	=	normal unit vector antiparallel to the track
P	=	bearing pressure
$\boldsymbol{Q}$	=	momentum of the mass sled
$\boldsymbol{R}$	=	sled radius vector $\|\boldsymbol{R}\| = R$
$\boldsymbol{r}$	=	gyration vector $\|\boldsymbol{r}\| = r$
s	=	displacement
t	=	time
$\boldsymbol{V}$	=	velocity $V = \sqrt{(\dot{x}^2 + \dot{y}^2)}$
$V_{/\!/}$	=	$\boldsymbol{n}$ of $\boldsymbol{V}$
$V_{\perp}$	=	$\boldsymbol{m}$ of $\boldsymbol{V}$
$\hat{\boldsymbol{V}}$	=	relative sled velocity
x	=	abscissa of sled
$\lfloor x \rfloor$	=	greatest integer $\leq x$
y	=	ordinate of sled
α	=	orientation angle, $\phi - 2\pi \lfloor (\phi/2\pi) \rfloor$, γ/R
γ	=	ratio of specific heats
δ	=	differences between upper and lower semicircle radii
Θ	=	integration variable
θ	=	lock-in angle
λ	=	radius of curvature
μ	=	coefficient of friction
ρ	=	diameter of circle
ϕ	=	orientation of $\boldsymbol{R}$
ψ	=	orientation of $\boldsymbol{r}$
ψ_0	=	initial value of ψ
$\|\|$	=	absolute value
$'$	=	$\mathrm{d}(\,)/\mathrm{d}\phi$
$\cdot$	=	$\mathrm{d}(\,)/\mathrm{d}t$
$\langle\,\rangle$	=	average value
$\times$	=	vector product

Introduction

A MECHANICAL method for accelerating a mass to high velocities via a device called the slingatron[1] has been proposed by Tidman.[1,2] Several slingatron configurations have previously been examined. For these configurations, the accelerated mass (called a sled in this report) interaction with the slingatron track was modeled with magnetic levitation[2] or with a mechanical friction force that is proportional to the normal force exerted by the track[1] on the sled. This report presents numerical simulations of slingatrons that have several different track configurations. The sled and track interaction is treated with a normal force friction model in which the friction coefficient μ is either a constant or an empirically determined function of the sled's velocity relative to the slingatron track.

These simulations reveal that the mass can be accelerated to very high velocities for each track configuration (track shape) examined here. Generally, the calculations show that spiral-shaped slingatrons will produce high velocities for constant gyration speeds, and the single-loop circular slingatron will produce high velocities when the gyration speed is increasing. We emphasize that the main reason this happens is that the sled locks into a constant phase angle as it transverses the slingatron track. When this occurs, the sled's velocity is optimally increased for each 2π revolution of the sled. This will continue until the frictional force dominates the component of the Coriolis force that is parallel to the slingatron track. However, there are cases with parameters chosen so that the parallel component of the Coriolis force is always greater than the force attributable to friction. In such cases, one will find that the nonrelativistic sled

Received 14 June 2001; revision received 20 September 2001; accepted for publication 15 October 2001.

*Research Physicist, Aerodynamics Branch. Senior Member AIAA.
†President, 6801 Benjamin Street. Senior Member AIAA.
‡Research Physicist, Aerodynamics Branch. Senior Member AIAA.

velocity increases indefinitely. For the spiral slingatrons, lock-in occurs almost instantaneously, whereas the circular slingatron requires significantly more time for lock-in to occur.

Theory

Figure 1 shows a sled of mass M moving along a track with position $\boldsymbol{R}+\boldsymbol{r}$ and a corresponding velocity $\boldsymbol{V}=\dot{\boldsymbol{R}}+\dot{\boldsymbol{r}}$. The sled's velocity is assumed to be large enough that it stays in contact with the track at all times. In fact, the velocity may be large enough to cause mass loss because of abrasion or evaporation, that is, $\dot{M}\neq 0$. The force $\boldsymbol{F}$ acting on the sled can be written as $\boldsymbol{F}=F_{\perp}\boldsymbol{m}+F_{/\!/}\boldsymbol{n}$ in which $\boldsymbol{m}$ and $\boldsymbol{n}$ are unit vectors pointing normal (toward the concave side of the track) and antiparallel to the track. Therefore, $\boldsymbol{n}=-\boldsymbol{R}'/R'$ and $\boldsymbol{m}=\boldsymbol{n}\times\boldsymbol{k}$ for unit vector $\boldsymbol{k}$, pointing out and normal to the plane of the track. Calling the unit vectors along the abscissa and ordinate $\boldsymbol{i}$ and $\boldsymbol{j}$ allows the momentum $\boldsymbol{Q}$, following Fig. 1, to be written as

$$\boldsymbol{Q}=M[\boldsymbol{k}\times(\dot{\phi}\boldsymbol{R}+\dot{\psi}\boldsymbol{r})+\dot{R}\boldsymbol{R}/R], \qquad \dot{\boldsymbol{Q}}=\boldsymbol{F} \tag{1}$$

The vectors $\boldsymbol{R}$ and $\boldsymbol{r}$ are expressed in Cartesian coordinates x and y of the $\boldsymbol{i}$, $\boldsymbol{j}$ plane so that

$$x=R\cos\phi+r\cos\psi, \qquad y=R\sin\phi+r\sin\psi \tag{2}$$

The parallel force $F_{/\!/}$ is assumed to be caused by friction, and, therefore, the standard friction model is assumed to have the form

$$F_{/\!/}=\mu(\hat{V})F_{\perp} \ni \hat{V}=|\dot{\phi}|\sqrt{R'^2+R^2} \tag{3}$$

for which $\hat{V}$ is the sled velocity relative to the track. Now, solving Eq. (1) for $F_{\perp}$ and $F_{/\!/}$ and then including Eqs. (2) and (3) results in the following differential equation:

$$\ddot{\phi}=-\frac{\dot{\phi}^2[\mu(R^2-RR''+2R'^2)+R'(R+R'')]}{R^2+R'^2}+\frac{\{[M(\ddot{\psi}+\mu\dot{\psi}^2)+\dot{M}\dot{\psi}]\sin(\psi-\phi)+[M\dot{\psi}^2-\mu(M\ddot{\psi}+\dot{M}\dot{\psi})]\cos(\psi-\phi)\}rR'}{M(R^2+R'^2)}$$
$$+\frac{\{[M(\dot{\psi}^2-\mu\ddot{\psi})-\mu\dot{M}\dot{\psi}]\sin(\psi-\phi)-[M(\ddot{\psi}+\mu\dot{\psi}^2)+\dot{M}\dot{\psi}]\cos(\psi-\phi)\}rR'}{M(R^2+R'^2)}-\frac{\dot{M}\dot{\phi}}{M} \tag{4}$$

Equation (4) is general enough to account for many slingatron configurations as long as the motion takes place in the $\boldsymbol{i}$, $\boldsymbol{j}$ plane. The configurations are obtained by the specification of the ϕ dependence of the vector $\boldsymbol{R}(\phi)$, which determines the shape of the slingatron track. The friction coefficient $\mu(\hat{V})$, the time dependent mass $M(t)$, and the gyration angle $\psi(t)$ must also be given to numerically integrate Eq. (4).

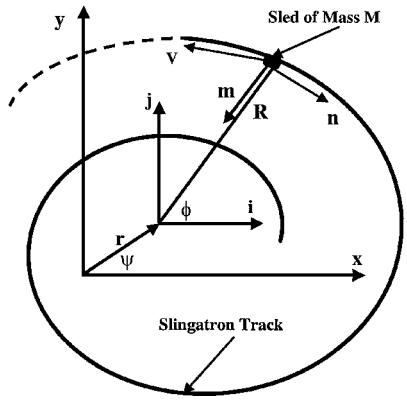

Fig. 1 Schematic of a general slingatron.

Circular Slingatron

This report considers several possible track configurations, all of which treat the length of the gyration arm, $|\boldsymbol{r}|=r$, as a constant. The first consideration is the circular slingatron[1,2] defined by

$$|\boldsymbol{R}(\phi)|=\text{const} \tag{5}$$

In general, we have found that any slingatron will optimally accelerate a sled to high velocities whenever the lock-in angle, $\theta=\psi-\phi$, is very close to constant, that is,

$$\dot{\theta}\approx 0 \text{ hence} \qquad \dot{\psi}\approx\dot{\phi}, \qquad \ddot{\psi}\approx\ddot{\phi} \tag{6}$$

Using the constraints given by Eqs. (5) and (6) simplifies Eq. (4) to the following expression:

$$\ddot{\phi}=b\dot{\phi}^2, \qquad b=\frac{r(\sin\theta-\mu\cos\theta)-\mu R}{r(\mu\sin\theta+\cos\theta)+R} \tag{7}$$

for constant μ and M. This is easily integrated to give us the sled's velocity $V=\sqrt{(\dot{x}^2+\dot{y}^2)}$ as

$$V=\frac{|\dot{\phi}(0)|\sqrt{2rR\cos\theta+R^2+r^2}}{|1-\dot{\phi}(0)bt|} \tag{8}$$

A plot of Eq. (8) is shown in Fig. 2 for $\theta=\pi/4$, $\phi(0)=0$, and $\dot{\phi}(0)=\pi$. One can see that the nonrelativistic velocity V becomes infinite at the time $t_{\infty}=1/\dot{\phi}(0)b$ whenever we force θ to be constant.[1,2] The values of t_{∞} change rapidly in regions where $\theta\approx\pi n$, $n=0, 1, 2, \ldots$, as given in Fig. 3. Equation (7) shows that $b=0$ whenever

$$\theta=\pm 2\tan^{-1}\left[\sqrt{(\alpha^2-1)\mu^2+\alpha^2}\mp\alpha/(\alpha-1)\mu\right]\pm\pi n$$
$$n=0, 1, 2 \tag{9}$$

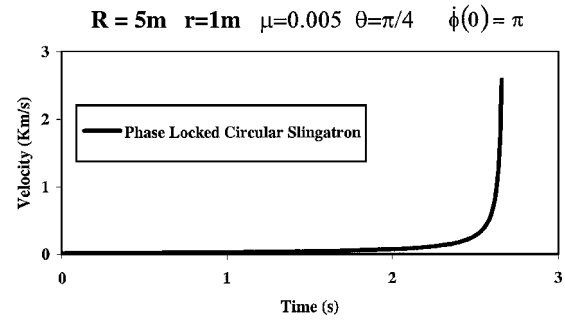

Fig. 2 Velocity vs time for the circular slingatron with phase lock-in.

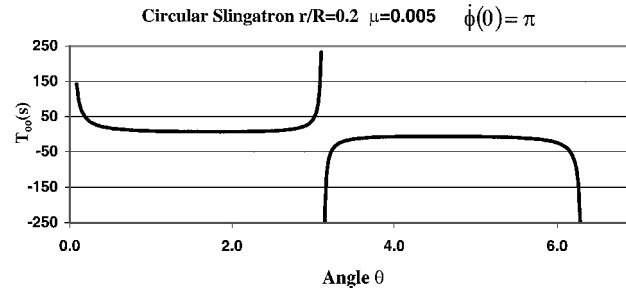

Fig. 3 Value of t_{∞} vs time for the circular slingatron.

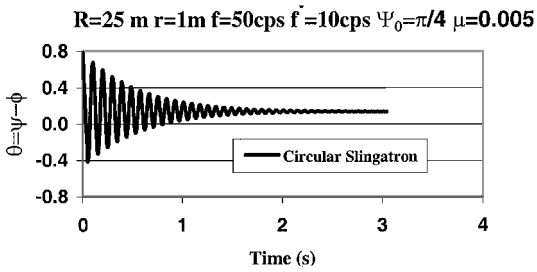

Fig. 4 Lock-in angle vs time for the circular slingatron.

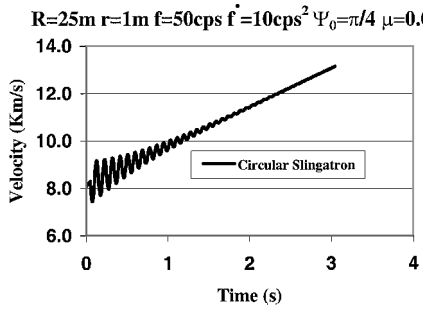

Fig. 5 Velocity vs time for the circular slingatron.

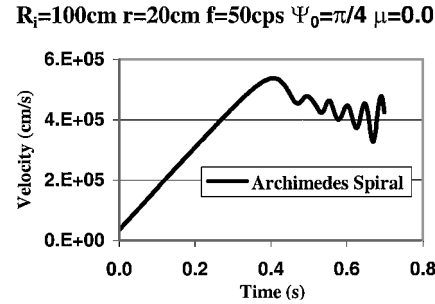

Fig. 6 Velocity vs time for the Archimedes spiral slingatron.

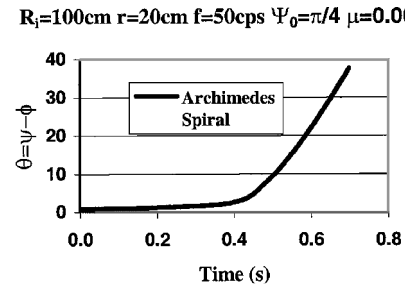

Fig. 7 Lock-in angle vs time for the Archimedes spiral slingatron.

assuming $(\alpha^2-1)\mu^2+\alpha^2 \geq 0$. These results used in Eq. (8) produce two time-independent velocities given by

$$V = \frac{\left|\dot{\phi}(0)\sqrt{(\alpha^2-1)\mu^2+\alpha^2} \mp 1\right|}{\sqrt{\mu^2+1}}$$

After a small amount of algebra, one will find that these constant velocities occur when the force attributable to friction is large enough to prevent the sled from accelerating along the circular track. Thus, the sled's velocity is constant.

Instead of demanding the constraints given by Eq. (6), let us consider an example of a circular slingatron with an accelerating angular gyration speed so that

$$\psi = \psi_0 + 2\pi f t + \pi \dot{f} t^2 \tag{10}$$

Numerically integrating Eq. (4), subject to Eq. (10), produces the velocity plot with initial conditions $\phi(0)=0$ and $\dot{\phi}(0)=2\pi f$ (Fig. 4). Here, we see that high velocities are obtained for $\dot{f} \neq 0$. The corresponding lock-in angle, $\theta = \psi - \phi$, given in Fig. 5 becomes relatively constant when sled velocities become large. Even though high sled velocities can be obtained with a circular slingatron, it is encumbered with the difficulty of creating an easy exit port for the high-speed sled. To alleviate this mechanical difficulty, we will next examine possible open-loop spiral slingatrons.

Archimedes Spiral Slingatron

We now focus our study on configurations that are not closed-loop slingatrons. In particular, we examine spiral-shaped tracks having open ends, which have the advantage of an easy exit for an accelerated sled entering free flight. Following Tidman,[1] we first examine an Archimedes spiral-shaped track given by

$$R = R_i + r\phi \sin\psi_0 \tag{11}$$

for which the constant R_i is the initial radius and spacing between adjacent spirals is determined by $\sin\psi_0$. The gyration speed is now held constant so that the expression given in Eq. (10) is replaced with

$$\psi = \psi_0 + 2\pi f t \tag{12}$$

Tidman[3] presents a first-order analysis for a sled with $\dot{M}=0$ and μ held constant. Putting Eq. (11) into Eq. (4) and keeping first-order terms, that is, in $\mathcal{O}(r/R, \mu)$, leads to the simple equation with $\theta = \psi - \phi$

$$V'/V = r\sin\theta/R(\phi) - \mu \tag{13}$$

Now, considering the change in velocity ΔV for the sled during a 2π revolution of a single spiral leads to the following expression for averaged quantities:

$$\Delta V/\text{cycle} \approx 2\pi\langle V\rangle[r\sin\theta/\langle R(\phi)\rangle - \mu] \tag{14}$$

This last expression suggests that spiral-shaped tracks can produce extremely high sled velocities for properly chosen $R(\phi)$. Equation (14) also shows that $R(\phi)$ may cause the ΔV/cycle to eventually become very small if the Coriolis force is balanced by friction.

Using Eq. (10) in Eq. (4), followed with numerical integration, allows us to produce the velocity plot, $V(t)=\sqrt{(\dot{x}^2+\dot{y}^2)}$, found in Fig. 6 for initial conditions $\phi(0)=0$ and $\dot{\phi}(0)=2\pi f$, that is,

$$V_{//}(0) = 2\pi f\left[\sqrt{R'^2+R^2} + r\cos(\tan^{-1}R'/R + \psi_0)\right]$$

and the sled mass held constant. We immediately see that the maximum velocity has the same order of magnitude as the circular slingatron (see Fig. 2) but does so in far less time and requires no acceleration of the gyration arm. The radius $R(\phi)$ changes so that the lock-in angle θ stays relatively constant until the sled has reached its maximum velocity, as seen when Fig. 6 is compared with Fig. 7. These plots also exemplify the discussion following Eq. (14) in which friction balances the parallel component of the Coriolis force as the sled moves along the spiral track. A plot presented in the following section provides further numerical confirmation of this conclusion.

Semicircle Slingatron

The next slingatron configuration examined is constructed with a sequence of semicircles having increasing radii (Fig. 8). We note that this slingatron continues to have the sled exit advantage found for the Archimedes slingatron. In fact, it may be easier to construct because constant radius semicircles now replace the continuously changing radius of the Archimedes spiral. This track has the added advantage in that large sled velocities can be obtained without the need of an initial sled injection, that is, $\phi(0)=0$ and

$$\dot{\phi}(0) = 0 \Rightarrow V_{//}(0) = 2\pi f r\cos(\tan^{-1}R'/R + \psi_0)$$

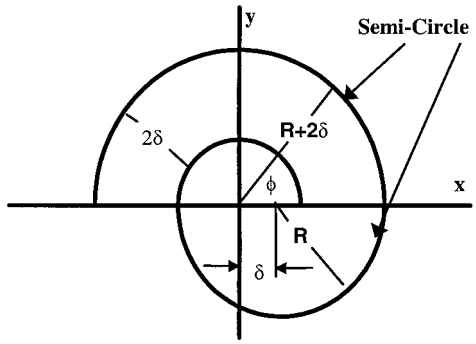

Fig. 8 Schematic of the semicircle slingatron.

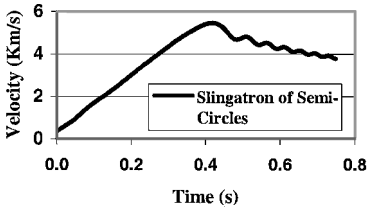

Fig. 9 Velocity vs time for the semicircle slingatron.

provided the slingatron has been scaled to a sufficiently large size. All of the previous slingatrons plus the small-scale high-frequency version of the present slingatron usually require the sled to have an initial injection velocity relative to the slingatron track $\phi(0)$ and $\dot{\phi}(0) \neq 0$, that is,

$$V_{//}(0) = \dot{\phi}(0)\sqrt{R'^2 + R^2} + 2\pi f r \cos(\tan^{-1} R'/R + \psi_0)$$

to obtain large maximum velocities. Because of these advantages, a more thorough investigation that includes sled pressure loads and an empirical friction model, incorporating mass loss $\dot{M} < 0$, is presented. According to Fig. 8, the semicircles in the upper half-plane are described by

$$R = R_i + 2\delta\lfloor\phi/2\pi\rfloor, \qquad R' = 0,$$
$$R'' = 0, \qquad \delta = \pi r \sin\psi_0 \tag{15}$$

and applying the law of cosines to this geometry, we find for the semicircles in the lower half-plane having center coordinates at $(\delta, 0)$ described as

$$R = \delta\cos\phi + \sqrt{(R_i + 2\delta\lfloor\phi/2\pi\rfloor + \delta)^2 - \delta^2\sin^2\phi}$$
$$R' = \frac{\delta R\sin\phi}{\delta\cos\phi - R}, \qquad R'' = \frac{R'^2 + 2\delta R'\sin\phi + \delta R\cos\phi}{\delta\cos\phi - R} \tag{16}$$

This definition shows that $R(\phi)$ is a monotonic (nondecreasing) function and, therefore, can cause plots of calculated parameters to exhibit small rippling effects. When the ripples were judged to detract from the overall intent of this report, computed data were smoothed using a moving average to minimize the rippling effects. Now, inserting Eqs. (15) and (16) into Eq. (4) and numerically integrating leads to sled velocities shown in Fig. 9. This high-frequency small-scale slingatron, that is, $f = 50$ cps and $R_i = 100$ cm, is subjected to initial conditions $\phi(0)$ and $\dot{\phi}(0) = 2\pi f$; we also assume that $\dot{M} = 0$ and $\mu = 0.005$. Figure 10 tells us again that the lock-in angle θ diverges from nearly a constant value, after the time t, when the sled reaches its maximum velocity.

An important simplification when one is constructing a semicircle slingatron occurs when we consider a large-scale version, that is, $f = 11$ cps and $R_i = 400$ cm, of this slingatron. For these cases, we can generate large maximum velocities without the need for an initial sled injection velocity $\hat{V} = 0$. An example of this is depicted in Fig. 11 so that $\phi(0) = 0$ and $\dot{\phi}(0) = 0$, and the sled mass as well as

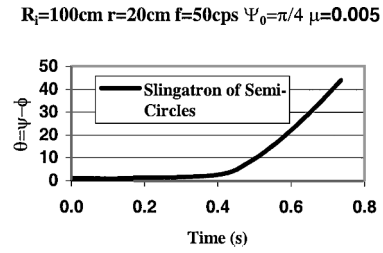

Fig. 10 Lock-in angle for the semicircle slingatron.

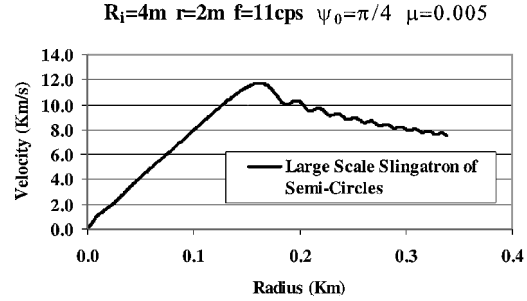

Fig. 11 Velocity vs radius for the semicircle slingatron.

the friction coefficient are held constant. This plot has the time axis replaced by radial distance to indicate the size of this large-scale example. In contrast, we note that the small-scale version of this slingatron still requires a nonzero initial sled velocity, $\dot{\phi}(0) \neq 0$, to obtain a significantly larger maximum sled velocity.

To address a more realistic slingatron, one should consider the interaction between the sled and the slingatron track. Therefore, we will assume that the sled is covered with material that abrades, $\dot{M} < 0$, as it moves along the track, in such a way that the removed mass acts as a lubricant. As the velocity increases, the abraded particles may become a liquid bearing, and at still greater velocities, the liquid will eventually evolve into a gas or even a plasma. To date, only a preliminary experimental investigation of the friction coefficient $\mu(\hat{V})$ dependence on the sled's relative speed $\hat{V}$ has been conducted by Tidman.[4] The preliminary data for a lexan sled indicate that

$$\mu(\hat{V}) = \frac{0.152}{(1 + 3.16\hat{V})}, \qquad \hat{V} = \dot{\phi}\sqrt{R'^2 + R^2} \tag{17}$$

in which $\hat{V}$ is measured in kilometers per second, ranging up to a maximum velocity of 4.0 km/s. The corresponding value of $\dot{M}$ is still very suspect, but the preliminary data give the following estimation:

$$\dot{M} = -\frac{M\hat{V}}{50\pi R(\phi)} \tag{18}$$

Tidman[1] has suggested that if the velocity (and, therefore, the bearing pressure between the track and the sled) is large enough to cause the abrading mass to become gaseous, one might then assume

$$\dot{M} = -\frac{\mu M\hat{V}}{\gamma(\gamma - 1)R(\phi)} \tag{19}$$

for lexan $\gamma \approx 1.25$. The two estimates found in Eqs. (18) and (19) are plotted in Fig. 12 under the assumption that the friction coefficient given by Eq. (17) is true for all velocities. Figure 13 shows the velocity results for a constant mass sled plus the two cases when $\dot{M} \neq 0$, given by Eqs. (18) and (19). Because there is no discernible difference among the three cases, we will select $\dot{M} = 0$ for the remainder of this paper. This selection should not be taken as a general conclusion because the present results stem from two simple $\dot{M}$ models. All that we can claim here is that the dynamics represented by Eq. (4) are weakly dependent on our two $\dot{M}$ models. A more in-depth study of the bearing physics may reveal that $\dot{M}$ cannot be ignored in a more elaborate friction model, and, therefore, $\dot{M}$ must be included in the momentum equations.

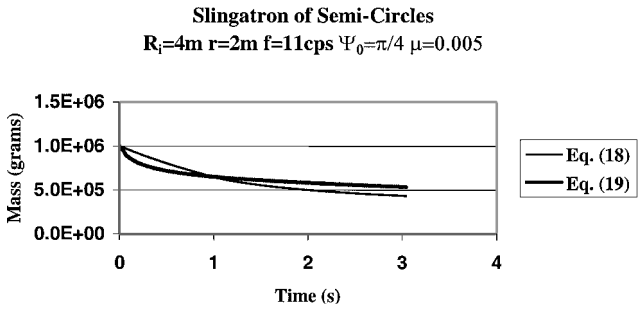

Fig. 12 Mass vs time for the semicircle slingatron.

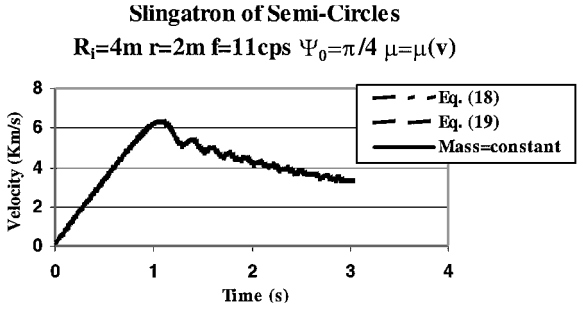

Fig. 13 Velocity comparison vs time as functions of M and $\dot{M}$.

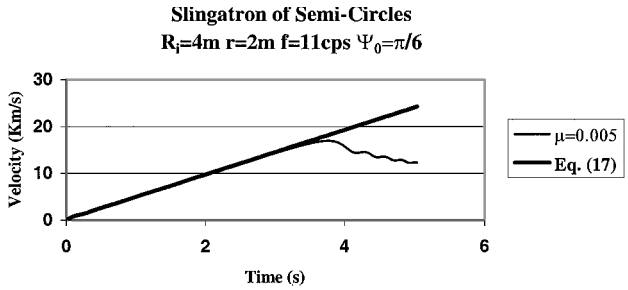

Fig. 14 Velocity comparison vs time as a function of μ.

To demonstrate the importance of the friction model, we next compare our empirical model, Eq. (17), to the constant friction model $\mu = 0.005$. Figure 14 has a sample comparison of the sled velocity with initial conditions $\phi(0) = 0$ and $\dot{\phi}(0) = 0$ for these two models. We see that Eq. (17) and the initial phase $\psi_0 = \pi/6$ can lead to classically unlimited velocities imparted to the sled. In this case, $\mu(\hat{V})$ decreases fast enough that the force attributable to friction never becomes great enough to overcome the parallel component of the Coriolis acceleration.

To gain insight into the magnitudes of the bearing pressure exerted by the sled on a semicircle slingatron, one can examine a typical right cylinder-shaped lexan-coated sled that has length L and diameter D. Assuming that the ablating material exerts a uniform pressure along the half lateral surface of the sled facing the slingatron track, one will find that the pressure

$$\mathrm{d}P = \frac{LD}{2\sin\Theta\,\mathrm{d}\Theta}$$

and integrating over the polar angle $0 \le \Theta \le \pi$ is easily calculated to be $P = F_{\perp}/DL$. An example of bearing pressure for a sled with initial mass $M = 1.0 \times 10^3$ kg, plotted as a function of time, is presented in Fig. 15.

Calculating the sled's acceleration along the unit vectors $\boldsymbol{m}$ and $\boldsymbol{n}$ while it traverses the slingatron track may also prove useful to the designer. Remembering that the normal component of the acceleration is always pointing toward the concave side of the track, we can find its magnitude from $A_{\perp} = \boldsymbol{A} \cdot \boldsymbol{m}$. An example of the large-scale slingatron is shown in Fig. 16. In a similar fashion, the parallel component of acceleration, $A_{/\!/} = -\boldsymbol{A} \cdot \boldsymbol{n}$, is plotted in Fig. 17 where, for

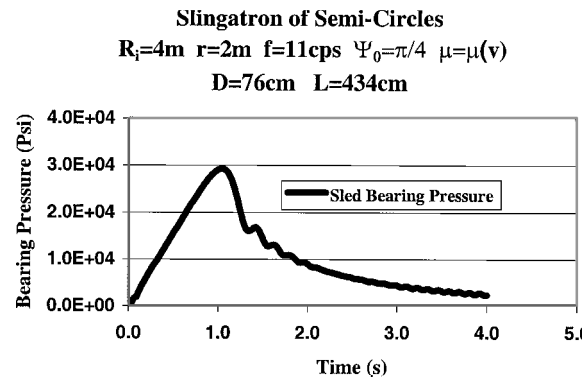

Fig. 15 Sled bearing pressure vs time for semicircle slingatron.

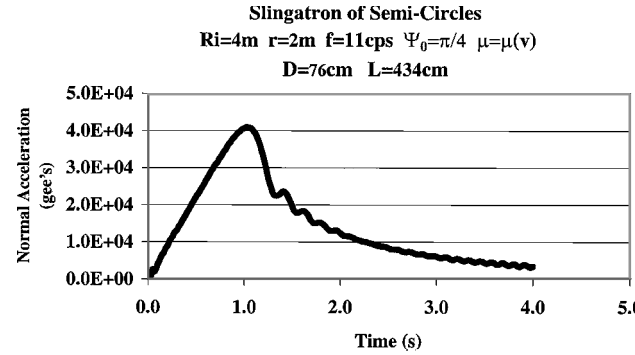

Fig. 16 Normal component of acceleration vs time for the semicircle slingatron.

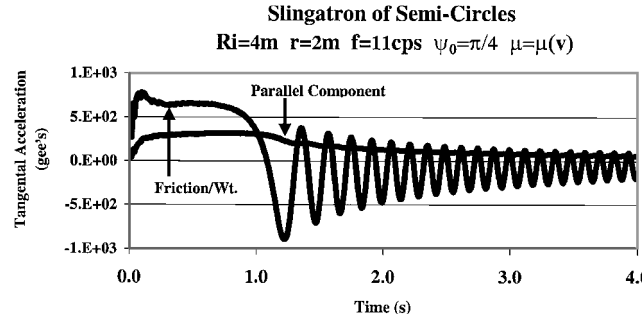

Fig. 17 Comparison of parallel component of acceleration and friction force/weight vs time.

comparison, we also plot $F_{\perp}/M$. Comparing Fig. 16 with Fig. 17 verifies that the time t where the maximum velocity is found is also the time where friction force per unit mass equals $A_{/\!/}$, thus substantiating the conclusion mentioned before.

Examining the curvature of the semicircle slingatron shows that $\boldsymbol{R}''$ is not continuous at the points, $\phi = n\pi$, $n = 0, 1, 2, \ldots$, where the upper half-plane semicircles meet the lower half-plane semicircles (see Eqs. (15) and (16)]. However, these discontinuities of the sled's acceleration are not severe enough to cause numerical integration problems of Eq. (4).

Further Illustrations

Before leaving the topic of spiral-shaped slingatrons, we present results for two other familiar spiral-shaped tracks. Both configurations have the nonzero initial velocity, $\phi(0) = 0$ and $\dot{\phi}(0) = 2\pi f$. The first is the parabolic spiral given by

$$R(\phi) = R_i + r\phi^2 \sin\psi_0 \tag{20}$$

A velocity plot for this is given in Fig. 18, for which the friction coefficient μ is modeled with Eq. (17). The last case considered is the logarithmic spiral, written as

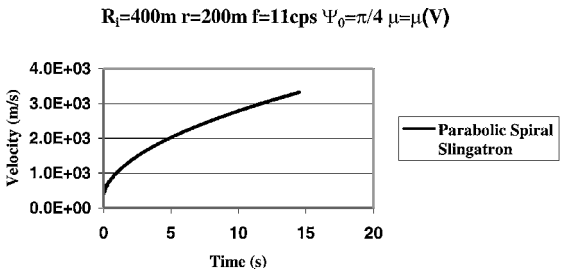

Fig. 18 Velocity vs time for the parabolic spiral slingatron.

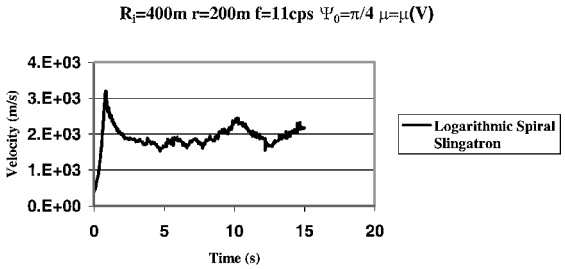

Fig. 19 Velocity vs time for the logarithmic spiral slingatron.

$$R(\phi) = R_i + r \sin \psi_0 \ln \phi \tag{21}$$

The velocity for this spiral is presented in Fig. 19 where, again, the coefficient μ is calculated with Eq. (17). One can see from Figs. 18 and 19 that a wide variety of choices for $R(\phi)$, r, $\dot{\psi}$, and f are possible to obtain large maximum sled velocities. These choices offer considerable flexibility when one is faced with design constraints for a spiral-shaped slingatron.

Conclusions

Circular slingatrons require the gyration arm r to accelerate, $\ddot{\psi} > 0$, for the mass sled to reach substantial maximum velocities. As time progresses, the sled is optimally accelerated as indicated by the lock-in angles θ approaching nearly a constant value. Experience from generated computer simulations for the closed circular slingatron reveal that initial sled velocities close to $\dot{\phi}(0) = 2\pi f$ are necessary to obtain large sled speeds.

The spiral slingatrons are able to produce sufficiently large maximum sled velocities with only constant angular gyration speeds, $\ddot{\psi} = 0$. Generally, spiral slingatrons require initial injection velocities in the neighborhood of $\dot{\phi}(0) = 2\pi f$ to gain large maximum sled speeds. However, there are exceptions for each spiral examined, such that sled velocities $\geq$8 km/s are possible when $\dot{\phi}(0) = 0$. The large-scale version of the semicircle slingatron generally produces high velocities, $\geq$8 km/s, for zero initial conditions. This favorable feature makes such slingatrons mechanically easier to build. Examination of the bearing pressure and the corresponding magnitude of the sled acceleration gives insight into the stress levels that the sled and spiral track must endure. In general, the sled acceleration parallel to the track shows that friction is the agent that limits the maximum sled speed. An empirical formula describing the friction force $\mu(\hat{V})$ shows that unlimited sled speeds are possible, in spite of friction, for the right choice of governing parameters.

There is a variety of choices regarding the spiral shape $R(\phi)$, as well as the parameters r, $\dot{\psi}$, ψ_0, and f, that one can use to produce a large range of maximum sled velocities. Even though the results given here strongly suggest that spiral-shaped tracks are the most desirable, the optimal spiral configuration is still an unanswered question. Experiments and further modeling to address the high-velocity dependence of $\mu(\hat{V})$ are slated to take place in the near future.

References

[1]Tidman, D. A., "Sling Launch of a Mass Using Superconducting Levitation," *IEEE Transactions on Magnetics*, Vol. 32, No. 1, 1996, pp. 240–247.

[2]Tidman, D. A., "Slingatron Mass Launchers," *Journal of Propulsion and Power*, Vol. 14, No. 4, 1998, pp. 537–544.

[3]Tidman, D. A., "Dynamics of the Spiral Slingatron," Advanced Launch Corp. TN ALC-1998-1.

[4]Tidman, D. A., "A Scientific Study on Sliding Friction Related to Slingatrons," UTRON Inc., Final Rept., U.S. Army Contract DAAD17-00-P-0710, Feb. 2001.